Pion-Proton Scattering below 150 Mev. II*

S. W. Barnes, H. Winick, K. Miyake, and K. Kinsey
University of Rochester, Rochester, New York

(Received July 16, 1959)

Values found for 30-Mev scattering at the two center-of-mass angles 116.8° and 155° are, respectively, for positive pions 0.849±0.048 and 1.098±0.075 mb sterad^{-1}, and for negative pions of the same energy 0.187±0.020 and 0.165±0.022 mb sterad^{-1}. Phase-shift analyses are made of recent published π^- distributions in the above energy range and serve to furnish prescriptions for the low-energy behavior of the $T=\frac{1}{2}$ phases. Calculations of σ^{--}, σ^{-0}, and $\sigma_{\text{total}}{}^-$ at various energies agree with measurements found in the literature. An essential agreement is found between π^-+p forward scattering amplitudes and a dispersion equation over this energy region.

I. DIFFERENTIAL CROSS-SECTION MEASUREMENTS AT 30 MEV

THE π^+ low-energy data used in Part I of this paper for phase-shift analysis were superior in quality and accuracy to the π^- information. A program to improve this situation was begun by Giacomelli[1] who measured the 30-Mev π^- elastic scattering at the two laboratory angles of 70.5° and 90°. We report below on the measurement of the scattering at the two angles 107.5° and 150° which serves to complete a rather sparse distribution at this energy.

The 107.5° point was obtained using the 70.5° equipment of Giacomelli rearranged to measure backward scattering. The geometry is shown in Fig. 1. The scattered pion pulse-height distribution of this run is quite broad as can be seen from Fig. 2 where the upper curve shows the π^+ distribution of 649 counts obtained from 20×10^6 incident counts with liquid hydrogen as well as the distribution of 64 counts for the same number of incident doubles with the target empty. The latter distribution is actually reckoned from 8.2×10^6 incident doubles in order to show a comparison between the full and empty counting rates. The lower pair of curves were observed in π^- scattering and correspond to 31×10^6 incident counts, giving 257 full and 62 empty scatterings.

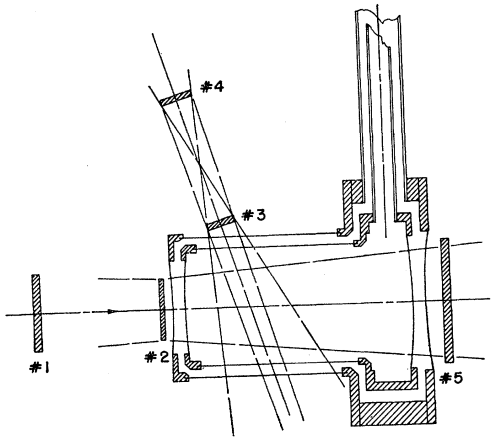

FIG. 1. Scattering geometry at 107.5°.

The corrections made to the full-empty count differences are listed in Table I. Usual corrections not shown were found to be negligible.

The solid angle averaged over the target area multiplied by the effective target thickness was calculated to be 0.417±0.008 steradian inch. The mean energy of this measurement was 29 Mev. The cross sections derived after the above corrections had been applied were further adjusted to correspond to a mean energy of 30 Mev by applying a correction of +3% to the π^+ and a correction of −4.4% to the π^- cross section. These corrections were arrived at by an iterative process: First a correction was made, based on the assumed energy dependency of the cross sections and a phase-shift solution was performed (see Sec. II). The energy dependence was then rederived and a new correction calculated. The corrections converged to the values given above.

The final values of the cross sections from these measurements are, in the c.m. system: $\theta=116.8°$, $d\sigma^+/d\Omega=0.849\pm0.048$ mb/sterad, $d\sigma^-/d\Omega=0.187\pm0.020$ mb/sterad.

Figure 3 shows the geometry of the 150° measurements. Since wall scattering could not be avoided at this angle it was minimized by moving the entrance and exit vacuum windows away from the scattering volume. The entrance window was mounted on the thin wall nose cone, close to crystal No. 2 where it could not be seen by the scattering telescope. The exit window was sufficiently far down stream to subtend a small solid angle at the scattering telescope. Since the anticoincidence crystal No. 5 had to be covered with a "proton stopper" (to prevent forward scattered protons from

TABLE I. Corrections to the data at 107.5°.

	π^-	π^+
Counts outside chosen channels	(+2.4±0.8)%	(+2.4±0.8)%
Beam contamination	(+11±3)%	(+3±1)%
Efficiency of scattering telescope	(+3±2)%	(+3±2)%
Incident randoms	(+1.5±0.5)%	(+1.5±0.5)%
Hydrogen vapor	(+1.5±0.5)%	(+1.5±0.5)%

* Supported in part by the U. S. Atomic Energy Commission.
[1] G. Giacomelli, this issue [Phys. Rev. **117**, 250 (1960)].

cancelling a backward pion), and this was thick compared to the hydrogen target, its contribution to the empty counts was reduced to a tolerable value by placing it even farther downstream in the pion beam.

The thickness of the hydrogen target was measured by sighting through two glass windows set in the vacuum wall with a traveling microscope. The measurements also located the center of the target with respect to the scattering telescope and so provided information for the calculation of its solid angle.

The measurement of the efficiency of the scattering telescope was done as follows. The telescope was mounted so it could be swung from the scattering position into a downstream position in the direct beam. An attenuator plate placed just before the telescope reduced the beam energy to the value expected for pions scattering at 150°. A small crystal No. 5 was

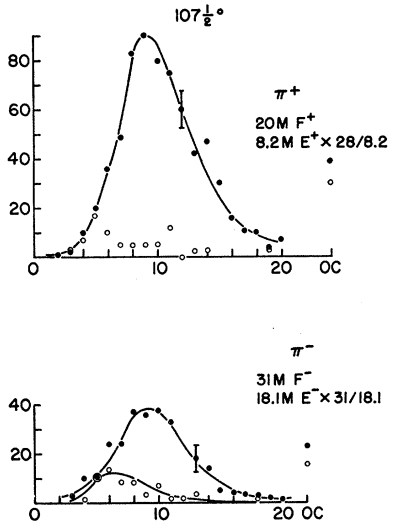

FIG. 2. Pulse-height distribution for pions scattered at 107.5°. Pions scattered with the target full are indicated by solid circles; with the target empty by open circles.

placed behind the telescope. The measurement of the ratio of 12345/125 then gave the detecting efficiency directly.

The energy and contamination of the incident beam was determined as described previously from a combination of range curves and pulse-height curves of crystal No. 2. The actual density of the beam over the target was found from vertical and horizontal traverse curves taken with a small crystal. Figure 4 shows, at the top, the observed π^+ distributions and the corresponding π^- distributions below. Two runs were made at this angle for which the important quantities are listed in Table II. Corrections not listed were negligible in terms of the over-all errors found below.

II. SOLUTIONS FOR THE $T=\frac{1}{2}$ PHASES

In Part I we found that all recent $\pi^+ + p$ total cross sections and differential distributions in the energy

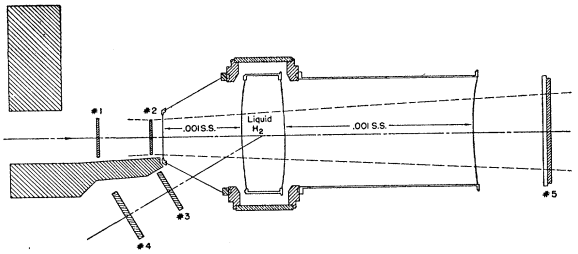

FIG. 3. Scattering geometry at 150°.

range of 25 to 150 Mev could be fitted if a certain set of scattering coefficients and certain energy dependencies were used in the usual s- and p-wave expressions for σ^{++} and $d\sigma^{++}/d\Omega$. These positive pion-proton data can then be considered to be internally consistent and suitable for combination with π^- elastic distributions measured anywhere in the above energy range. The separate π^- distributions we have used in this way are those of Ashkin *et al.*[2] at 170 and 150 Mev, that of Holt *et al.*[3] at 98 Mev, the π^- distribution at 41.5 Mev reported in Part I, and the 30-Mev π^- distribution made up of the data of Giacomelli and of the preceding section.

The results of the analyses are given in Table III. The first row indicates by the energy figure the particular π^- distribution which is combined with the combination of π^+ distributions referred to as Combination D in part I. The last two columns give, respectively, the partial χ^2 which indicates the goodness of fit to the π^- distribution and the expected value of this χ^2. The values of χ^2 in parentheses are the values quoted by Ashkin[2] and Holt.[3] On line 1 are listed the values of the $T=\frac{3}{2}$ coefficients found in this analysis. They are the same for all solutions and were previously given on

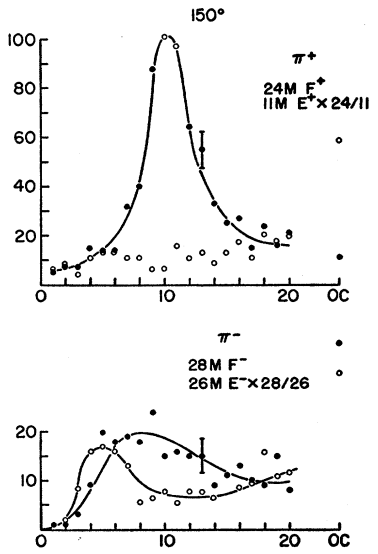

FIG. 4. Pulse-height distribution for pions scattered at 150°. Pions scattered with the target full are indicated by solid circles; with the target empty by open circles.

[2] Ashkin, Blaser, Feiner, and Stern, Phys. Rev. **101**, 1149 (1956).
[3] Edwards, Frank, and Holt (to be published).

TABLE II. 150° scattering results and corrections to data for two runs.

	Run 1		Run 2	
	π^+	π^-	π^+	π^-
Incident counts, target full	24×10^6	55×10^6	8×10^6	26×10^6
Scattered counts, target full	577	306	250	191
Incident counts, target empty	11×10^6	49×10^6	5.6×10^6	20.4×10^6
Scattered counts, target empty	59	167	36	82
Contamination	3±1%	6±2%	4±2%	11±4%
Efficiency	86±5%		95±4%	
Outside channels	3±1%		...	
Solid angle	0.1886±0.0056 sterad		0.238±0.007 sterad	
Mean scattering angle c.m.	153.3°		155.0°	
Target thickness	3.23±0.03 cm		3.23±0.03 cm	
Mean energy	31.2±2.0 Mev		31.6±2.0 Mev	
Energy correction	0.96	1.06	0.94	1.07
$d\sigma/d\Omega_{c.m.}$ at 30 Mev (in mb/sterad)	1.12±0.10	0.15±0.03	1.08±0.11	0.183±0.036
Weighted average of two runs	$d\sigma^+/d\Omega=1.098+0.075$ mb/sterad		$d\sigma^-/d\Omega=0.165+0.022$ mb/sterad	

the last line of Table IV, Part I. The succeeding lines with the exception of the lowest show the values found at each energy for the $T=\frac{1}{2}$ coefficients. The errors ascribed to the values of α_1^N, α_{11}^N, and α_{13}^N of Table III for the energies of 170, 150, and 98 Mev arise from the nonsystematic errors of the measured differential cross sections. Since systematic errors are also reported for these data, the errors of Table III are underestimates. The effect of the systematic errors was examined at each of these energies by repeating the analysis with the π^- differential cross sections for one energy shifted first up, then down, by the amount of the appropriate systematic error. The results were that the errors ascribed to α_1^N and α_{11}^N were essentially unchanged at any of the three energies while there was a notable increase in the range of values of α_{13} at the two energies of 170 and 150 Mev. This is indicated in Fig. 5 where the short bars above and below the statistical error markers indicate maximum and minimum values for the phases which are permitted by the inclusion of the systematic errors. It is quite possible that this finding is related to the method of analysis.

The last line of the table needs some remarks and they follow. The values for the phases found in the 41.5- and 30-Mev analyses are reasonably consistent but are associated with woefully large errors which occur principally because of the paucity of points in each distribution. A two-energy combination solution of these data would presumably yield smaller errors and could be made if $T=\frac{1}{2}$ phase shift momentum dependencies were known. Since they were not known, they were approximated by making plots of the Table III values of each phase shift against momentum and drawing reasonably shaped smooth curves through the points. Inspection of these curves showed that the phases could be represented over this narrow momentum interval quite satisfactorily by the following simple expressions:

$$\alpha_1^N=\eta^{\frac{1}{2}}a_1';\quad \alpha_{11}^N=\eta a_{11}';\quad \alpha_{13}^N=\eta a_{13}'.$$

The primed constants had values which yielded phase shift values corresponding to the midpoints of the smooth curves. With these dependencies the machine found a solution for the total of 9 π^- differential cross sections at 41.5 and 30 Mev, and these phase shifts appear in the last line. Their errors are enclosed in parentheses since they are affected by assumptions as to energy dependencies while other errors (of $T=\frac{1}{2}$ phases) in the table are not.

It should also be noted that the Table III values of χ^2 indicate that the 170-, 150-, and 98-Mev distributions are rather poorly fitted. We find the goodness of fit to be essentially unchanged when the data are increased or decreased by the amount of the reported systematic error.

TABLE III. Results of phase-shift analysis for various combinations of data.

Combination	a_{31}^N	a_3^N	f^2	χ^2 (observed)	χ^2 (expected)
D	−0.0418+0.0044	−0.1145+0.0026	+0.0877+0.0014	21.25	33
	α_1^N	α_{11}^N	α_{13}^N		
D+170 π^-	0.164 ±0.014	−0.006 ±0.022	0.057 ±0.010	8.9 (9.7)[a]	5
D+150 π^-	0.147 ±0.008	−0.012 ±0.012	0.031 ±0.006	18.8 (14.4)[a]	5
D+98 π^-	0.134 ±0.003	−0.021 ±0.004	−0.004 ±0.003	19.35 (18.9)[b]	10
D+41.5 π^-	0.121 ±0.015	−0.006 ±0.037	−0.016 ±0.020	0.774	2
D+30 π^-	0.115 ±0.014	0.002 ±0.110	−0.015 ±0.050	0.710	1
D+35.75 π^-	0.114 (±0.004)	0.001 (±0.025)	−0.017 (±0.012)	0.977 at 30 Mev	1
				0.955 at 41.5 Mev	2

[a] Quoted by Ashkin *et al.* See reference 2.
[b] Quoted by Holt *et al.* See reference 3.

TABLE IV. Comparison of quantities calculated from phase shifts with experimental values.

	Calc.	Exp.	Calc.	Exp.	Calc.	Exp.
	20 Mev		30 Mev		41.5 Mev	
σ^{--}	1.9		2.14 ±0.14		1.83 ±0.17	
σ^{-0}	6.0	5.0 ±0.8[a]	6.8 ±0.5	5.7 ±0.9[a]	7.04 ±0.59	6.9±1.2[a]
$\sigma_{\text{total}}^{-}$	8.0		9.0 ±0.5		8.87 ±0.47	
D_{-}^{b}			0.10 ±0.01		0.108±0.009	
	98 Mev		120 Mev		144 Mev	
σ^{--}	6.1 ±0.2	6.15 ±0.22[b]	11.4	11.3 ±1.6[c]	18.8	17.0±2.4[c]
σ^{-0}	14.9 ±0.6	15.0 ±0.8[b]	23.1		34.4	
$\sigma_{\text{total}}^{-}$	21.1 ±0.8	21.9 ±0.7[b]	34.5	{33.4 ±3.2[c] 38 ±9[e]	53.2	{48.1±4.5[e] 55 ±6[e]
D_{-}^{b}	0.206±0.004[d]	0.195±0.006[b]			0.261	
	150 Mev		170 Mev			
σ^{--}	20.2 ±1.0	20.01 ±1.57[f]	23.9 ±1.8	23.5 ±1.8[f]		
σ^{-0}	37.4 ±2.0	34.6 ±2.9[f]	43.3 ±2.6	39.0 ±3.3[f]		
$\sigma_{\text{total}}^{-}$	57.6 ±2.2	55.3 ±1.6[e,f]	67.2 ±2.7	62.7 ±1.9[e,f]		
D_{-}^{b}	0.24 ±0.01[d]	0.260±0.021[g]	0.194±0.015[d]	0.227±0.032[g]		

[a] W. J. Spry, Phys. Rev. **95**, 1295 (1954).
[b] See reference 3.
[c] Anderson, Fermi, Martin, and Nagle, Phys. Rev. **91**, 155 (1953).
[d] Reported systematic errors are not included.
[e] Attenuation measurement.
[f] See reference 2.
[g] Calculated by H. Schnitzer and G. Salzman, Phys. Rev. **112**, 1802 (1958).

In Fig. 6 are plotted the experimental differential cross sections together with smooth curves calculated from the phase shifts reported in Table III.

III. TESTS OF THE PHASE SHIFTS OF TABLE III

Table III values of the phase shifts for the four energies 33.75, 98, 150, and 170 Mev are plotted in Fig. 5. The curves connecting the points are drawn to please the eye. A polynomial expression for $\alpha_1=(0.205\eta-0.09\eta^3+0.018\eta^5)$ represents the α_1 curve of Fig. 5 but errors cannot be given for the coefficients.

Using the phase shifts of Table III and phase shift values from the curves of Fig. 5 for other energies various quantities were calculated and listed in Table IV. Errors are given for the quantities if the phases come from Table III but are omitted if the phases were picked from the curves of Fig. 6. Cross sections are given in millibarns while the values of D_{-}^{b} are, as usual, in units of $\hbar/m_\pi c$. The first column under each energy heading contains calculated numbers while those to the right are experimental values reported by the authors referred to.

The table shows agreement where comparison can be made between calculated and measured cross sections. In view of the considerable errors $\sigma_{\text{total}}^{-}$ is reported as the sum of the elastic and charge exchange cross sections—the radiative capture cross section being ignored. It appears then that the assumptions made as to (1) the value of r_0, (2) the value of ω_0^*, (3) s- and p-wave analysis, and (4) exact charge independence, are satisfactory for the explanation of the data at

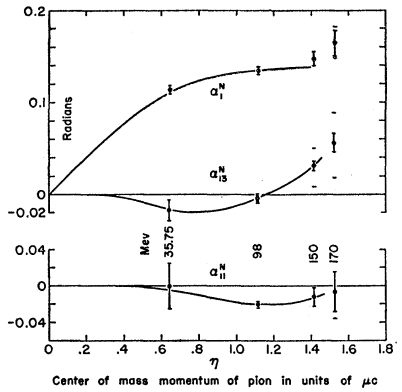

FIG. 5. $T=\frac{1}{2}$ phase shifts as a function of momentum. The smooth curves have been drawn to please the eye.

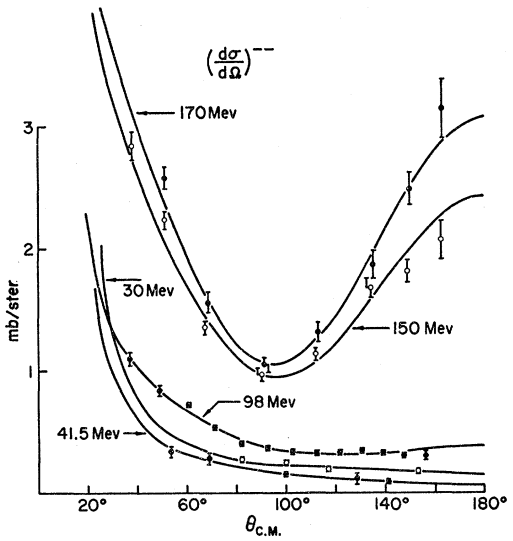

FIG. 6. π^- experimental differential cross sections with smooth curves calculated from phase shifts of Table III.

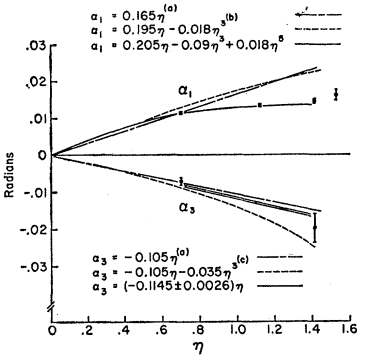

FIG. 7. S-wave phase shifts compared with various prescriptions. (a) J. Orear, Nuovo cimento 4, 856 (1956); (b) H. L. Anderson, *Proceedings of the Sixth Annual Rochester Conference on High-Energy Nuclear Physics, 1956* (Interscience Publishers, New York, 1956); (c) Ferrari *et al.*, *Proceedings of the CERN Symposium on High-Energy Accelerators and Pion Physics, Geneva, 1956* (European Organization of Nuclear Research, Geneva, 1956).

present in hand (in this energy range) concerning pion-proton scattering cross sections.

Various prescriptions have been advanced for the behavior of the s phases at low energy. Some of these are shown in Fig. 7. The values we obtain clearly rule against the first two listed for α_1 but show no strong preference for any of the three listed for α_3.

It is of interest to inspect the discrepancy, first pointed out by Puppi and Stanghellini,[4] between $\pi^- + p$ forward scattering amplitudes and the predictions of dispersion theory. This has been recently reviewed by Schnitzer and Salzman,[5] among others, and we will make comparisons with their conclusions. Their Fig. 3 contains a separate graph of the value of each of the five terms of the π^- dispersion equation as a function of the laboratory kinetic energy of the pion. Their two terms representing the integral of positive pion total cross sections we accept without alteration since the low-energy parts of both total cross-section curves which they use are in agreement with values we find. The other three terms contain, respectively, the values 0.165 for a_1, -0.105 for a_3, and 0.08 for f^2. When these are replaced by the following values which we prefer: $a_1 = 0.205$, $a_3 = -0.114$, and $f^2 = 0.088$, and the curves are replotted, they sum to give the solid curve of Fig. 8. For comparison the broken line is the curve of Schnitzer and Salzman while the open circles represent the original curve of Puppi and Stanghellini.

The experimental points shown at the energies of 30, 41.5, 98, 150, and 170 Mev are taken from Table IV. The error markers of the 98-, 150-, and 170-Mev points are derived without inclusion of effects of systematic errors. Inspection of the table shows that the value we ascribe to $D_-{}^b$ at 98 Mev is about one standard deviation larger than the value Holt reports, while our values at 150 and 170 Mev are about one standard deviation smaller than the values derived by Schnitzer and Salzman from the distributions measured by Ashkin. The 220-Mev point is transcribed from the paper of the above two authors while the point at 307 Mev is taken from Geffen.[6] It is evident that none of the curves of Fig. 8 fits all of the data. The solid curve touches the four lower energy points but misses the three at higher energy. However, there now exists agreement rather than a discrepancy over at least a limited energy range (30 to 150 Mev) between experiment and $D_+{}^b$ (see Part I) and $D_-{}^b$ dispersion relations which are computed with common values of f^2, s-wave scattering lengths and $\sigma_{\text{total}}{}^+$ and $\sigma_{\text{total}}{}^-$ distributions.

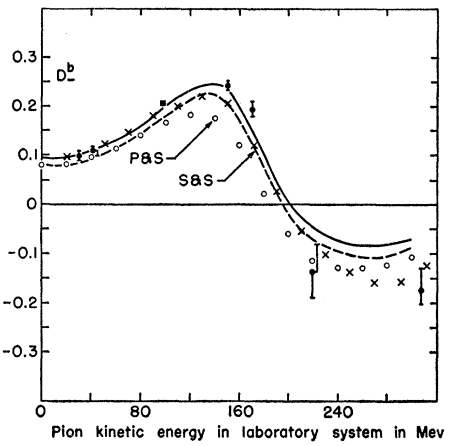

FIG. 8. $D_-{}^b$ *vs* incident pion energy—experimental points (with error brackets) compared to dispersion theory. The solid curve is computed from data of Schnitzer and Salzman using new values of a_1, a_3, and f^2. The broken curve is that of Schnitzer and Salzman (see reference 5). The open circles are the curve of Puppi and Stanghellini[4] and the crosses are the curve of Geffen.[6]

ACKNOWLEDGMENTS

We acknowledge gratefully the assistance of Mr. Alex Wieber who helped in the design of and carried the responsibility for the set up and alignment of the various scattering assemblies. We are indebted to Mr. Dave Knapp for assistance during the runs and to Mr. Fred Palmer and his crew for many hours of cyclotron operation.

Note added in proof.—The rather large value of $(a_1 - a_3)$ found above is judged to be due principally to the large value we find for a_1. A more nearly linear momentum dependence than we have found for α_1 would reduce a_1. Such a dependence is perhaps indicated by the values of α_1 reported in the 200- to 300-Mev region by S. M. Korenchenko and V. G. Zinov.[7] However, their errors are not small and the values they find for other phases, in particular α_3 and α_{31}, are in some disagreement with those recently reported from Berkeley[8] at a comparable energy.

[4] G. Puppi and A. Stanghellini, Nuovo cimento **5**, 1256 (1957).
[5] H. Schnitzer and G. Salzman, Phys. Rev. **112**, 1802 (1958).
[6] D. A. Geffen, Phys. Rev. **112**, 1371 (1958).
[7] B. Pontecorvo in *1959 Annual International Conference on High Energy Physics* (Interscience Publishers, New York, 1959).
[8] J. H. Foote, O. Chamberlain, E. H. Rodgers, H. M. Steiner, C. Wiegand, and T. Ypsilantis, Phys. Rev. Letters **4**, 30 (1960).